membranes

Article

Combining Arrhenius Modeling and Residual Machine Learning for Predicting Hydrogen Permeability in Pd–Cu Membranes

Hatem M. Alsyouri [1,*], Farqad Al-Hadeethi [2], Eldhose Iype [3] and Malyuba A. Abu-Daabes [4]

[1] Chemical Engineering Department, School of Engineering, The University of Jordan, Amman 11942, Jordan
[2] Chemical Engineering Department, Faculty of Engineering and Natural Sciences, Uskudar University, 34662 Uskudar, Istanbul, Türkiye; farqad.alhadeethi@uskudar.edu.tr
[3] College of Engineering and Technology, American University of the Middle East, Egaila 54200, Kuwait; eldhose.iype@aum.edu.kw
[4] Pharmaceutical and Chemical Engineering Department, German Jordanian University, Amman 11180, Jordan; malyuba.abudaabes@gju.edu.jo
* Correspondence: alsyouri@ju.edu.jo; Tel.: +962-(79)-989-9199

Abstract

Hydrogen permeability is a key parameter for Pd–Cu membrane design and evaluation. Although Arrhenius-type expressions are widely used to describe the temperature dependence of permeability, existing models often represent membrane-related effects indirectly through fitted transport parameters and are commonly developed for specific systems or operating conditions. To address this challenge, an Arrhenius-based delta machine-learning approach was developed to predict hydrogen permeability in Pd–Cu membranes using a literature-derived database of 266 permeability measurements. An Arrhenius model was used to describe the temperature dependence of hydrogen permeability and provide a baseline prediction. Residual analysis was then used to identify permeability variability not captured by the Arrhenius model and define a residual (delta) term. The residual term was modeled using Linear Regression and Kernel Ridge Regression (KRR) based on membrane composition, geometry, thickness, phase, and operating-condition variables. The Arrhenius model yielded a mean absolute percentage error (MAPE) in permeability of 123.4%, indicating that temperature alone could not fully describe permeability variability. Linear Regression reduced MAPE to 99.9%, while KRR reduced it to 32.15%. Combining Arrhenius transport modeling with delta machine-learning residual prediction improved permeability prediction across the Pd–Cu membrane dataset. The approach may support future studies integrating permeability prediction with degradation and durability analyses.

Keywords: hydrogen permeability; Pd–Cu membranes; Arrhenius modeling; hybrid modeling; physics-guided machine learning; Kernel Ridge regression; delta learning

Academic Editor: Diogo M.F. Santos

Received: 24 October 2026
Revised: 19 November 2026
Accepted: 23 November 2026
Published: 28 November 2026

Copyright: © 2026 by the authors. Licensee MDPI, Basel, Switzerland. This article is an open access article distributed under the terms and conditions of the Creative Commons Attribution (CC BY) license.

1. Introduction

Hydrogen is widely recognized as a promising clean energy carrier for supporting the transition toward sustainable energy systems. Green hydrogen, produced by water electrolysis using renewable electricity, offers an environmentally friendly pathway for reducing carbon emissions. However, the hydrogen-rich gas stream generated during electrolysis contains impurities that must be removed before the hydrogen can be used

in applications requiring high purity, such as Proton Exchange Membrane Fuel Cells (PEMFCs) and other advanced energy systems [1].

Dense metallic membranes, particularly palladium (Pd) and Pd-based alloys such as Pd–Cu, are among the most effective technologies for hydrogen purification. These membranes selectively permeate hydrogen while rejecting other gases, enabling the production of high-purity hydrogen with excellent separation performance [2]. As a result, Pd-based membranes have received considerable attention for hydrogen purification units integrated with PEMFC systems and other hydrogen-energy applications [3].

In practical applications, Pd–Cu membranes must maintain not only high hydrogen permeability but also adequate long-term durability. Previous studies have shown that Pd–Cu systems are susceptible to degradation mechanisms, including galvanic corrosion under aggressive operating conditions, which can promote membrane deterioration and reduce service life [4]. Consequently, the development of Pd–Cu membranes requires consideration of both hydrogen transport performance and long-term durability. In our previous work, the galvanic corrosion behavior of Pd–Cu couples was investigated experimentally and described using mathematical modeling under different operating conditions [5]. While that study focused on membrane degradation and durability, the present work addresses the complementary problem of hydrogen permeability prediction.

Hydrogen permeability in Pd and Pd-alloy membranes has been investigated using empirical Arrhenius correlations that describe its temperature dependence [6,7], mechanistic transport models based on solution-diffusion and Sieverts-law formulations [8,9], thermodynamic and atomistic analyses [10], and reactor-scale numerical simulations [11] . These approaches have improved the understanding of hydrogen transport in Pd-based membranes and have demonstrated that permeability depends on alloy composition, crystal phase, microstructure, thermal history, and operating conditions [12–14]. Nevertheless, membrane-related effects are often represented indirectly through fitted transport parameters rather than incorporated explicitly as predictive variables. For example, variations in alloy composition and phase structure have been reflected through differences in activation energies reported in Arrhenius-type permeability correlations [7,12,13], while composition-dependent changes in diffusivity and solubility, together with phase-dependent effects on hydrogen transport behavior and solubility, have also been reported [15,16]. Similarly, pressure exponents in Sieverts-type expressions have been associated with transport mechanisms, surface effects, and membrane thickness [4,17,18]. In addition, many permeability models have been developed for specific membrane compositions, phase regions, reactor configurations, or operating ranges [11,19]. Consequently, predicting hydrogen permeability across diverse Pd–Cu membranes, particularly when multiple membrane characteristics and operating variables vary simultaneously, remains challenging.

These limitations motivate the development of predictive approaches that combine physically based transport descriptions with data-driven methods that incorporate membrane descriptors directly.

Data-driven approaches have attracted increasing interest in membrane science as tools for prediction, material screening, and design. Machine-learning models have been applied to predict gas permeability in polymeric membranes and to assist the identification of promising membrane materials [20,21]. Similar approaches have also been used in high-throughput screening studies of metal–organic frameworks (MOFs) for hydrogen separation [22]. More recently, data-driven methods have been explored for the design and optimization of palladium-based membranes for hydrogen purification [23–25]. Existing machine approaches may be broadly categorized as purely data-driven models,

which predict permeability directly from selected input variables, and hybrid approaches that combine physical descriptions with machine learning. Purely data-driven models can provide flexibility in capturing complex relationships among variables [20,21,26], but they do not explicitly incorporate physical transport descriptions. Hybrid approaches, on the other hand, provide an opportunity to retain established transport descriptions while using machine learning to represent permeability variations not captured by conventional models [23,27].

Despite the potential advantages of hybrid approaches, applications combining physically based transport descriptions with machine learning for hydrogen permeability prediction in Pd–Cu membranes remain limited, particularly across datasets spanning different membrane compositions, phases, geometries, thicknesses, and operating conditions.

To address this challenge, the present work develops an Arrhenius-based residual (delta) machine-learning [28] framework for predicting hydrogen permeability in Pd–Cu alloy membranes. A literature-derived database containing hydrogen permeability measurements together with membrane characteristics and operating conditions was used to develop predictive models based on Linear Regression and Kernel Ridge Regression (KRR). The Arrhenius equation was first used to provide a physically meaningful baseline description of the temperature dependence of hydrogen transport. Machine-learning models were then employed to predict the residual permeability variations associated with membrane composition, geometry, thickness, phase, and operating conditions that were not explicitly represented by the Arrhenius model. The resulting framework combines the physical basis of conventional transport correlations with the flexibility of data-driven modeling and was evaluated against the conventional Arrhenius formulation using a literature-derived dataset covering a range of Pd–Cu membrane compositions and operating conditions.

2. Materials and Methods

2.1. Research Framework

The overall methodology consists of three stages: compilation of a literature-derived permeability dataset, development of an Arrhenius-based baseline model, and construction of residual machine-learning models. The Arrhenius formulation was first used to describe the temperature dependence of hydrogen permeability and provide a physically based baseline prediction. Residual permeability variations not represented by the Arrhenius model were then modeled using Linear Regression and Kernel Ridge Regression (KRR) as functions of membrane characteristics and operating conditions to improve prediction accuracy. The resulting framework combines conventional transport modeling with data-driven prediction.

2.2. Literature-Derived Dataset

A literature-derived dataset was assembled from published studies reporting hydrogen permeability measurements for Pd–Cu alloy membranes. The dataset was compiled to capture variations in permeability associated with membrane characteristics and operating conditions that have been reported to influence hydrogen transport. The selected variables included alloy composition, crystal phase, membrane geometry, membrane thickness, and operating temperature. The resulting dataset forms the basis for the development and evaluation of the predictive models.

Hydrogen permeability data for Pd–Cu alloy membranes were collected from carefully selected literature sources relevant to the objectives of this study [16,29–34]. Table 1 summarizes the variables considered and their corresponding ranges. More than 350 ob-

servations were initially compiled, including both permeability and permeance measurements. To maintain consistency across the dataset, only permeability data were retained, resulting in a final dataset of 266 observations.

Table 1. Summary of variables included in the literature-derived dataset.

Variable	Type	Range
Hydrogen permeability (Q)	Membrane characteristic	Literature values
Temperature	Operating condition	79–625 °C
Membrane thickness	Membrane characteristic	1.5–102 μm
Membrane geometry	Membrane characteristic	Supported foil, unsupported foil, composite membrane, supported thin film
Pd content	Membrane characteristic	45–100%
Cu content	Membrane characteristic	0–55%
Third metal	Membrane characteristic	0–3.9%
Alloy phase	Membrane characteristic	FCC, BCC, mixed

Hydrogen permeability values were extracted from tables, text, and graphical data reported in the selected references. For each observation, the corresponding membrane temperature, geometry, thickness, alloy composition, and phase structure were recorded when reported in the original source. The compiled dataset was subsequently screened to identify and remove duplicated observations that may have resulted from repeated reporting in multiple references. Observations with different input variables were retained as independent data points, even when similar permeability values were reported.

Since the dataset was assembled from multiple literature sources, experimental systems varied among studies. Nevertheless, hydrogen permeability measurements generally followed similar operating principles and membrane-test configurations. A representative experimental arrangement used for permeability measurements in Pd-alloy membranes is shown in Figure 1.

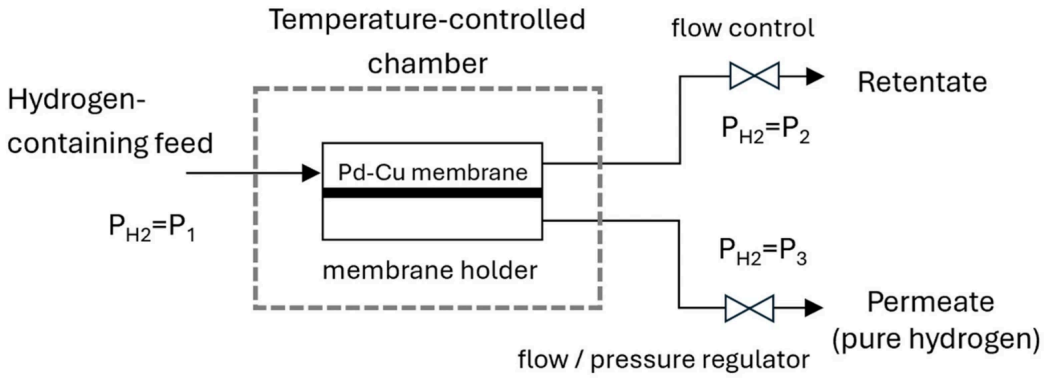

Figure 1. Generalized experimental apparatus for measuring flux and permeation. P_i denotes the hydrogen partial pressure at the feed (P_1), retentate (P_2), and permeate (P_3) sides.

Hydrogen transport through Pd-alloy membranes is typically investigated using a membrane module housed within a temperature-controlled chamber. The membrane separates feed and permeate compartments, and hydrogen permeates through the dense metallic layer under a controlled transmembrane hydrogen pressure difference. Feed, retentate, and permeate flow rates are monitored during operation, while pressure and

temperature are controlled throughout the experiment. Hydrogen purity is commonly determined using gas chromatography.

2.3. Data Processing and Modeling

The collected permeability data were processed to develop predictive models for hydrogen transport in Pd–Cu membranes. Hydrogen permeability was represented using the natural logarithm of permeability, ln(Q), as the modeling target, consistent with the linearized form of the Arrhenius equation. A conventional Arrhenius-based description was first employed to establish a baseline representation of the temperature dependence of hydrogen permeability. Subsequently, machine-learning models were developed to account for permeability variations associated with membrane characteristics and operating conditions and to improve prediction accuracy.

Although the Arrhenius model captures the dominant influence of temperature on hydrogen permeability, additional variability remains due to membrane composition, crystal phase, geometry, thickness, and other membrane characteristics. A residual term (Δ) was therefore defined as the difference between the experimental and Arrhenius-predicted values of ln(*Q*). The residual term represents permeability variations associated with membrane characteristics and operating conditions that are not explicitly captured by the Arrhenius temperature dependence. Rather than replacing the Arrhenius formulation, the residual-learning approach was used to model this remaining variability. This strategy retains the physical basis of Arrhenius transport modeling while incorporating membrane descriptors as explicit predictive variables.

Linear Regression was first employed as a baseline machine-learning model to evaluate the extent to which the permeability residuals (Δ) could be represented using linear relationships between the selected features and the target variable. The feature set included inverse temperature, membrane geometry, thickness, Pd mass fraction, Cu mass fraction, third metal mass fraction and crystal phase, while the target variable corresponded to the permeability residual (Δ). Non-numerical features are converted to numbers according to the index of the first instance each value appears in the array. No scaling is used. In the linear model, the target value (y) is expressed as a linear combination of the input features (x_i) weighted by model coefficients (w_i), $y = \sum_{i=1}^{n} w_i x_i$, where n is the number of input features. The model coefficients were determined during training by minimizing the mean absolute error (MAE) between predicted and observed values.

To account for potential nonlinear interactions among membrane properties and operating conditions, Kernel Ridge Regression (KRR) was subsequently used. KRR is a robust machine-learning technique that has been widely applied in regression problems and is particularly suitable for relatively small datasets [35]. KRR combines ridge regression with kernel-based feature transformation, enabling more complex relationships to be represented than those captured by conventional linear regression. Among several available kernel functions, the radial basis function (RBF) kernel was selected and is defined as

$$k\left(x, \tilde{x}\right) = e^{\left(-\gamma \left| x - \tilde{x} \right|^2\right)} \quad (1)$$

where x represents the training input, $\tilde{x}$ represents the prediction input, and γ is related

to the kernel width parameter σ according to $\gamma = \frac{1}{2\sigma^2}$

The KRR model also incorporates a regularization parameter (α) that controls model complexity and helps mitigate overfitting. The hyperparameters γ and α were optimized using a grid-search procedure prior to model development, resulting in optimal values of $\gamma = 1.0$ and $\alpha = 1 \times 10^{-10}$.

The predictive performance of the developed models was assessed using the mean absolute percentage error (MAPE), which is calculated as

$$MAPE = \frac{100\,\%}{n} \sum_{n} \frac{\left| y_{predicted} - y_{experiment} \right|}{\left| y_{experiment} \right|} \quad (2)$$

Since the machine-learning models were trained using ln(Q) as the target variable, MAPE values were first evaluated on the logarithmic permeability scale. For practical interpretation, predicted ln(Q) values were subsequently transformed back to permeability values (Q), and corresponding MAPE values were also calculated on the original permeability scale. Model generalization was assessed using learning curves, five-fold cross-validation, and the leave-one-out method. The resulting performance metrics were used to compare the predictive capabilities of the Arrhenius, Linear Regression, and KRR models.

All data processing, modeling, and visualizations were implemented in Python (v3.11) using pandas (v1.5.3), NumPy (v1.24.3), scikit-learn (v1.3), and Matplotlib (v3.7.1). The compiled literature dataset and Python analysis scripts are provided in the Supplementary Materials.

3. Results and Discussion

3.1. Fundamentals of Hydrogen Transport in Pd-Alloy Membranes

Pd and Pd-alloy membranes are widely used for hydrogen purification due to their ability to selectively permeate hydrogen while rejecting other gases. The hydrogen permeation mechanism in Pd-based membranes is illustrated in Figure 2 and involves adsorption of hydrogen molecules on the membrane surface (Step 1), followed by dissociation into atomic hydrogen (Step 2). The hydrogen atoms subsequently dissolve into the metallic lattice (Step 3), diffuse through the membrane bulk (Step 4), and precipitate on the permeate-side surface (Step 5). The atoms then recombine to form hydrogen molecules (Step 6), which are desorbed into the gas phase (Step 7) [36]. Under typical operating conditions, particularly at temperatures above 200°C and for sufficiently thick membranes (over 10 μm), diffusion through the bulk metal (Step 4) is generally considered the rate-limiting step, while the remaining processes may be assumed to be in dynamic equilibrium.

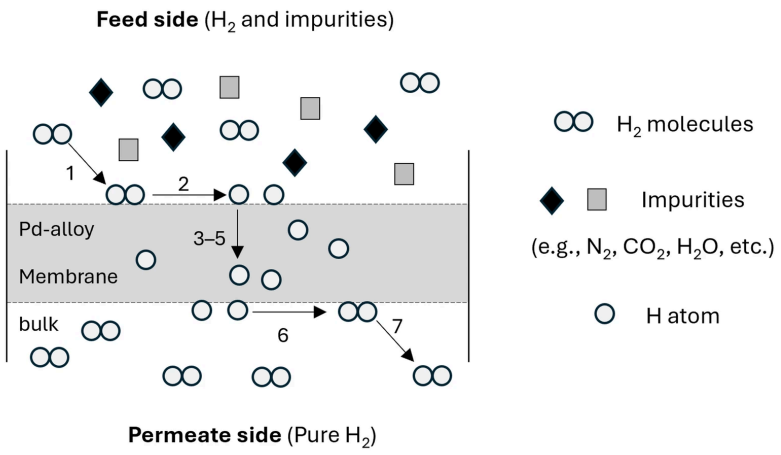

Figure 2. Schematic of hydrogen permeation through Pd-based membranes.

Under diffusion-controlled conditions, hydrogen permeation through Pd-alloy membranes is commonly described using Sieverts-type relationships derived from Fick's law and hydrogen solubility in the metal lattice [32,33,37]. The hydrogen flux through the membrane may be expressed as

$$J_{H2} = \frac{D_H \cdot K_S}{l} \left({P_h}^n - {P_l}^n \right) \quad (3)$$

where J_{H2} is the hydrogen flux, D_H is the hydrogen diffusion coefficient, K_S is the hydrogen solubility constant, l is the metallic membrane thickness, and P_h and P_l are the hydrogen partial pressures on the feed and the permeate sides respectively. The pressure exponent n reflects the dominant transport mechanism and is typically close to 0.5 for dense Pd-alloy membranes under diffusion-controlled conditions. Deviations from this value may occur due to membrane defects, mass-transfer limitations, support effects, or other transport contributions associated with membrane structure and operating conditions [32].

In the membrane literature, the product of the diffusion coefficient (D_H) and solubility constant (K_S) is commonly represented by the membrane permeability (Q) [9,37] leading to

$$J_{H2} = \frac{Q}{l} \left({P_h}^n - {P_l}^n \right) \quad (4)$$

When membrane thickness cannot be accurately defined, such as for metallic films deposited within porous supports, permeance (Q') (') is often reported instead, where $Q' = Q / l$.

Since the present work aims to develop predictive models for membrane permeability, only permeability data were retained during dataset compilation to ensure consistency among the collected literature sources.

Both hydrogen diffusivity and solubility are temperature-dependent and have been reported to vary with alloy composition and crystal structure [15,16]. Consequently, membrane permeability (Q) is commonly described using the Arrhenius relationship:

$$Q = Q_0 \ Exp\left(-\frac{E_a}{R}\ \frac{1}{T}\right) \quad (5)$$

where Q_0 is the pre-exponential factor, E_a is the activation energy for permeation, R is the universal gas constant, and T is the absolute temperature. The parameters Q_0 and E_a are commonly obtained from permeability measurements and have been reported to vary with alloy composition, phase structure, and membrane microstructure [12–14]. According to this relationship, the natural logarithm of permeability ($\ln Q$) exhibits a linear dependence on inverse temperature ($1/T$) . Although the Arrhenius model provides a useful description of the temperature dependence of hydrogen permeability, additional factors such as membrane composition, geometry, thickness, and phase may also influence transport behavior. These effects are investigated through the data-driven modeling approaches developed in the present work.

3.2. Arrhenius-Based Analysis of Hydrogen Permeability

The Arrhenius relationship is widely used to describe the temperature dependence of hydrogen permeability in metallic membranes, as it reflects the thermally activated nature of hydrogen diffusion and dissolution within the membrane material. Consequently, the Arrhenius model is commonly employed as a first approximation for correlating hydrogen permeability with temperature. In the present study, the Arrhenius model was used as a baseline framework for evaluating the permeability behavior of the compiled Pd–Cu membrane dataset.

Figure 3 compares the literature permeability data with the corresponding Arrhenius fit by plotting the natural logarithm of permeability, ln(Q), as a function of inverse temperature ($1/T$). The Arrhenius-fit values were calculated from the Arrhenius correlation presented in Equation (5) and therefore describe the temperature-dependent permeability predicted by the fitted Arrhenius model against the dataset. The literature permeability data exhibit an overall Arrhenius-type trend, confirming the expected dependence of hydrogen permeability on temperature. However, significant scatter and multiple clusters of data points are observed around the fitted Arrhenius trend. The Arrhenius model yielded a mean absolute percentage error (MAPE) of 3.08% on the ln(Q) scale. When transformed back to the original permeability scale, the corresponding MAPE was 123.43%, indicating that temperature alone could not fully describe the permeability variability present within the dataset.

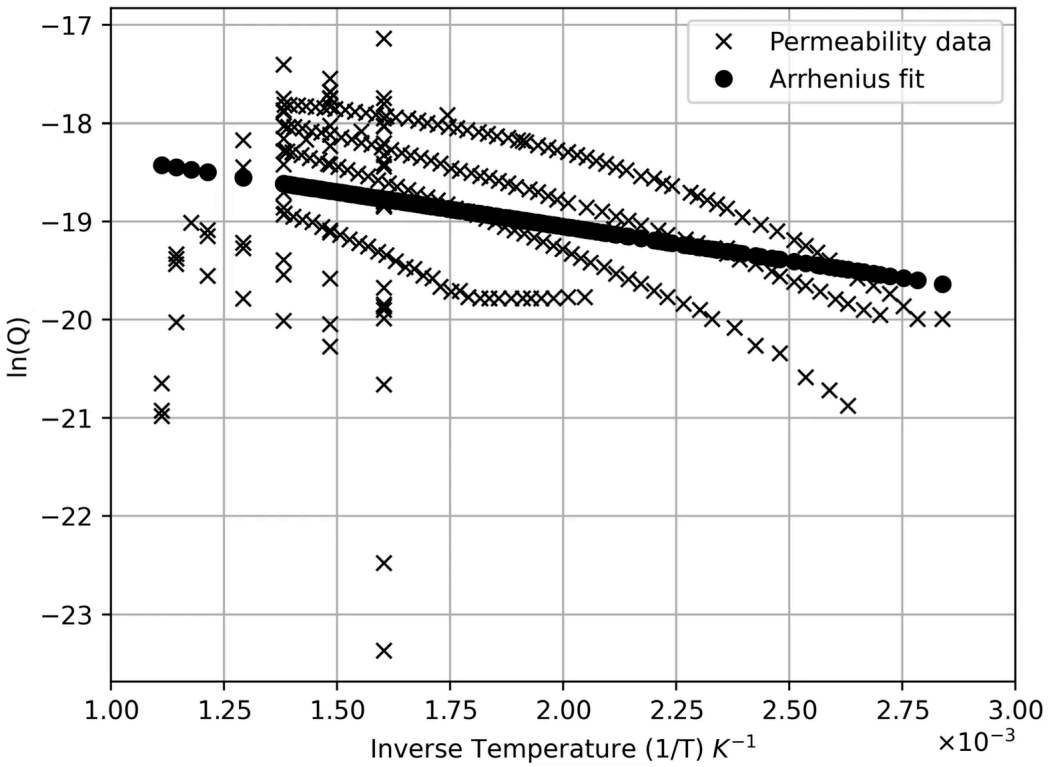

Figure 3. Comparison between literature permeability data and the Arrhenius-based model.

The distribution of the permeability data around the Arrhenius fit provides further insight into the limitations of the temperature-only description. Rather than being randomly scattered around the fitted correlation, several clusters of data points appear above and below the Arrhenius trend, indicating that membranes operating under similar temperatures may still exhibit substantially different permeability values. This behavior suggests that additional membrane characteristics influence permeability and that a single Arrhenius relationship is insufficient to fully describe the variability present within the literature-derived dataset.

To further investigate the origin of these deviations, the residual term (Δ), defined as the difference between the experimental and Arrhenius-predicted values of ln(Q), was analyzed as a function of selected membrane characteristics. The resulting residual distributions are presented in Figure 4. For an ideal Arrhenius description, the residuals would exhibit random scatter around zero with no systematic dependence on the remaining variables. In such a case, temperature alone would adequately describe the permeability behavior. However, Figure 4 reveals that the residuals are not randomly distributed and exhibit distinct patterns with respect to several membrane characteristics, indicating that additional factors influence permeability beyond the temperature dependence.

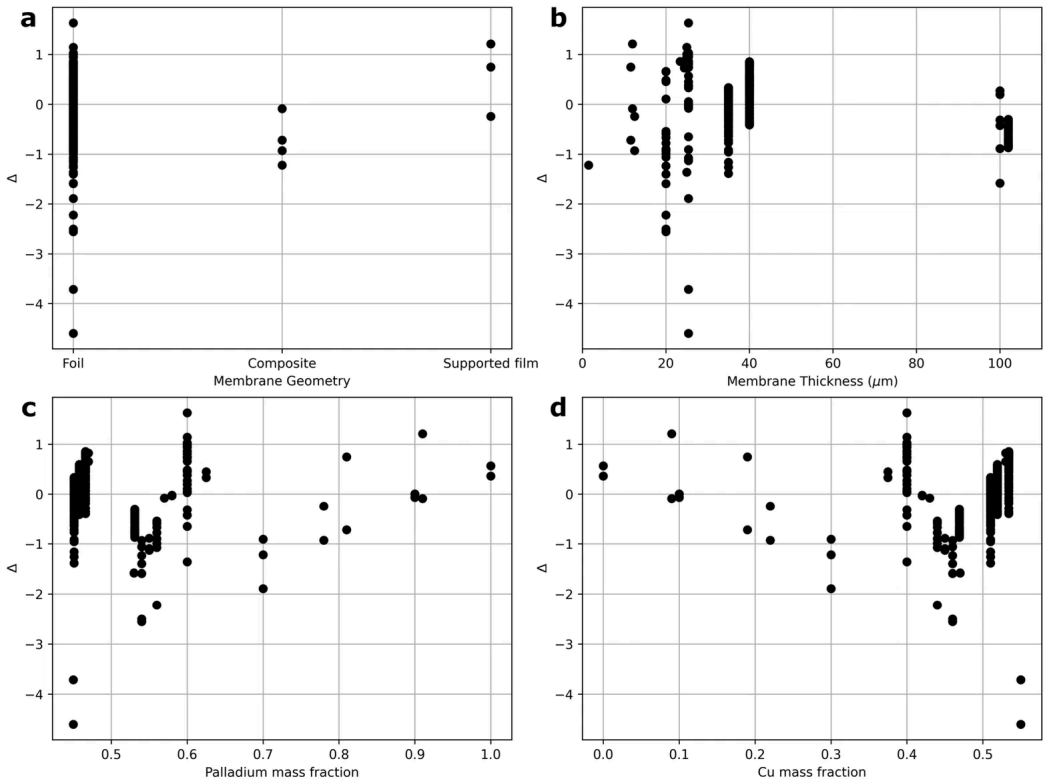

Figure 4. Permeability residuals (Δ) after Arrhenius fitting vs. selected membrane parameters (features): (**a**) residual vs. membrane geometry; (**b**) residuals vs. membrane thickness; (**c**) residuals vs. Palladium mass fraction; (**d**) residuals vs. Copper mass fraction.

The residual plots also provide insight into the relative influence of the investigated variables. Membrane geometry exhibits clustered residual distributions associated with different membrane configurations, although a clear trend is not evident. Similarly, membrane thickness displays a non-random distribution of residual values, suggesting that thickness contributes to permeability variability through a relationship more complex than a simple linear dependence. More pronounced patterns are observed for alloy composition, where both Pd and Cu mass fractions exhibit systematic variations in residual values across the investigated composition range. These observations indicate that alloy composition exerts a significant influence on permeability and contributes to the variability not captured by the Arrhenius model.

The residual distributions shown in Figure 4 may also be interpreted in terms of physical phenomena affecting hydrogen transport in Pd–Cu membranes. The residuals do not represent a single mechanism; rather, they reflect permeability variations arising from multiple membrane-related factors beyond the temperature dependence. Previous studies have shown that hydrogen transport in Pd–Cu membranes is sensitive to phase structure. For example, Martin et al. [15] reported substantially different hydrogen solubilities for FCC and BCC Pd–Cu structures, while Nayebossadri et al. [16] demonstrated that hydrogen permeability depends on the combined effect of phase structure, hydrogen diffusivity, and hydrogen solubility. Phase-transition effects may also contribute to the residual behavior. Yuan et al. [19] observed permeation hysteresis within the FCC/BCC miscibility region, while Goldbach et al. [12] reported structural and compositional segregation during cycling through this phase-transition regime, leading to heterogeneous membrane structures and changes in permeability. Consequently, the residual term may reflect phase-related effects on hydrogen transport that are not explicitly

represented by the Arrhenius temperature dependence.

Overall, the Arrhenius analysis demonstrates that temperature is a dominant factor governing hydrogen permeation in Pd–Cu membranes, but it is not sufficient to fully describe the variability present within the literature-derived dataset. The residual analysis further confirms that membrane composition, geometry, thickness, and phase introduce additional complexity that is not captured by a single temperature-dependent correlation. These findings motivate the use of multivariable machine-learning models capable of simultaneously incorporating the combined effects of multiple membrane characteristics and operating conditions to improve permeability prediction.

3.3. Linear Regression Modeling of Permeability Residuals

The residual analysis presented in Figure 4 demonstrated that hydrogen permeability is influenced by factors beyond temperature alone. To account for these effects, a Linear Regression model was developed within a physics inspired Δ-learning framework using seven input features: inverse temperature, membrane geometry, membrane thickness, Pd mass fraction, Cu mass fraction, third-metal mass fraction, and alloy phase. The Linear Regression model was trained to predict the residual term $\Delta = ln(Q)_{exp} - ln(Q)_{Arrh}$, corresponding to the portion of permeability not explained by the Arrhenius correlation. The final permeability prediction, $ln(Q)_{pred}$, was then obtained by combining the Arrhenius baseline prediction, $ln(Q)_{Arrh}$, with the residual correction predicted by the Linear Regression model, Δ_{pred}.

Figure 5 compares the performance of the Linear Regression model with the experimental permeability data and the Arrhenius baseline. In the upper plot, the Arrhenius fit (green crosses) represents the permeability predicted solely from the temperature-dependent correlation described by Equation (5). The Linear Regression predictions (black crosses) were obtained by applying the predicted residual corrections to the Arrhenius baseline. Compared with the Arrhenius model, the Linear Regression predictions exhibit improved agreement with the experimental permeability data and begin to reproduce part of the spread and clustering observed within the dataset. This behavior indicates that the additional membrane characteristics identified in the residual analysis contain meaningful information that contributes to hydrogen permeability prediction.

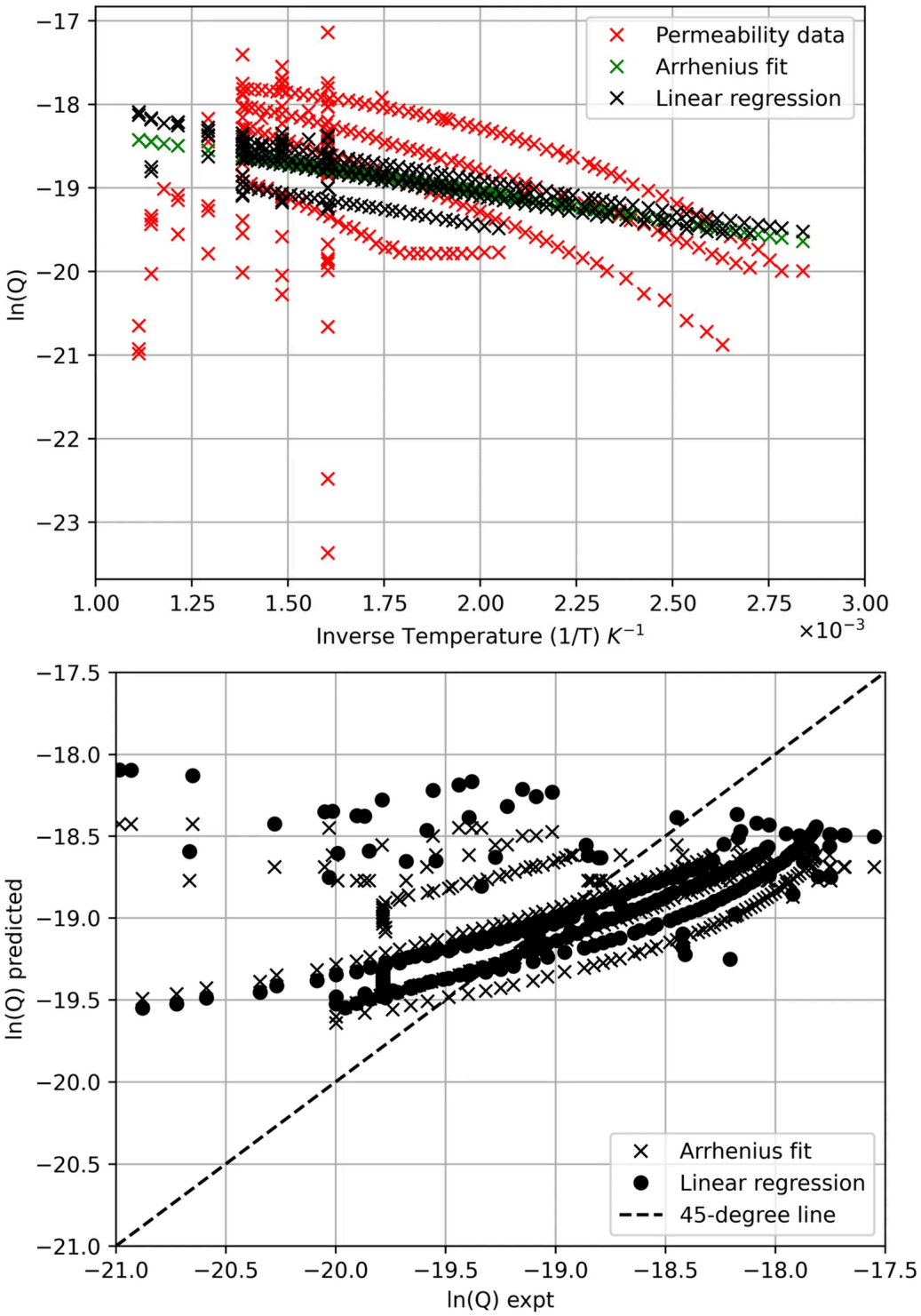

Figure 5. Linear regression model: (**upper**) model comparison with original data and Arrhenius plot; (**lower**) predicted vs. actual ln permeability plots.

The improvement achieved by the Linear Regression model is further illustrated in the lower plot of Figure 5, where the predicted and experimental permeability values are compared directly. For an ideal predictive model, all data points would lie on a parity line (y = x), where the predicted and experimental values match exactly. Relative to the Arrhenius model, the Linear Regression predictions are distributed closer to this ideal relationship, indicating improved predictive capability. This improvement is reflected by a reduction in the MAPE on the permeability scale from 123.4% for the Arrhenius model

to 99.9% for the Linear Regression model. On the ln(Q) scale, the corresponding MAPE was reduced from 3.08% to 2.79%. The reduction in prediction error confirms that incorporating membrane characteristics improves the description of permeability compared with a temperature-only correlation.

Despite this improvement, noticeable scatter remains in the parity plot and significant deviations from the ideal relationship can still be observed. Furthermore, the Linear Regression model does not fully reproduce the complete spread of the experimental permeability values, indicating that a portion of the dataset variability remains unexplained. These results suggest the presence of nonlinear interactions among membrane composition, geometry, thickness, phase, and temperature-related effects that cannot be fully captured by linear combinations of the selected variables. Therefore, a more flexible nonlinear regression approach is investigated in the following section.

3.4. Kernel Ridge Regression (KRR) Modeling of Permeability Residuals

Building upon the Arrhenius-based residual-learning framework, KRR was employed to capture the nonlinear interactions contributing to hydrogen permeability. Unlike Linear Regression, which assumes linear relationships between the input variables and the residual term, KRR provides a more flexible description of the residual contribution by representing complex nonlinear interactions among the membrane characteristics (features) and permeability residuals. As described in the methodology, the KRR model was trained to predict the residual term, $\Delta = ln(Q)_{exp} - ln(Q)_{Arrh}$, using membrane characteristics and operating-condition (inverse temperature) features. The final permeability prediction was obtained by combining the Arrhenius baseline prediction with the residual correction predicted by the KRR model according to $ln(Q)_{pred} = ln(Q)_{Arrh} + \Delta_{pred}$.

KRR utilizes a Radial Basis Function (RBF) kernel, $k(x, x')$, to quantify the similarity between membrane features in the multidimensional feature space. The behavior of the model is controlled by the kernel width parameter (σ) and regularization parameter (α), which determine the flexibility and generalization capability of the model. These hyperparameters were optimized using a grid-search procedure, resulting in optimal values of $\gamma = 1.0$ and $\alpha = 1 \times 10^{-10}$. The optimized KRR model was subsequently used to predict the residual correction, Δ_{pred}, for each permeability observation.

Figure 6 compares the KRR predictions with the experimental permeability data and the Arrhenius baseline. In the upper plot, the Arrhenius fit (green crosses) represents the permeability predicted solely from the temperature-dependent correlation of Equation (5), whereas the KRR predictions (black crosses) represent the Arrhenius prediction corrected using the physics inspired Δ-learning model with 'the kernel trick' [38]. Compared with the Linear Regression results shown in Figure 5, the KRR model reproduces the experimental permeability distribution more accurately and better captures the spread of permeability values observed throughout the dataset. The multiple permeability levels previously identified in Figure 3 are also represented more effectively, indicating that nonlinear relationships among the selected variables contribute significantly to permeability behavior.

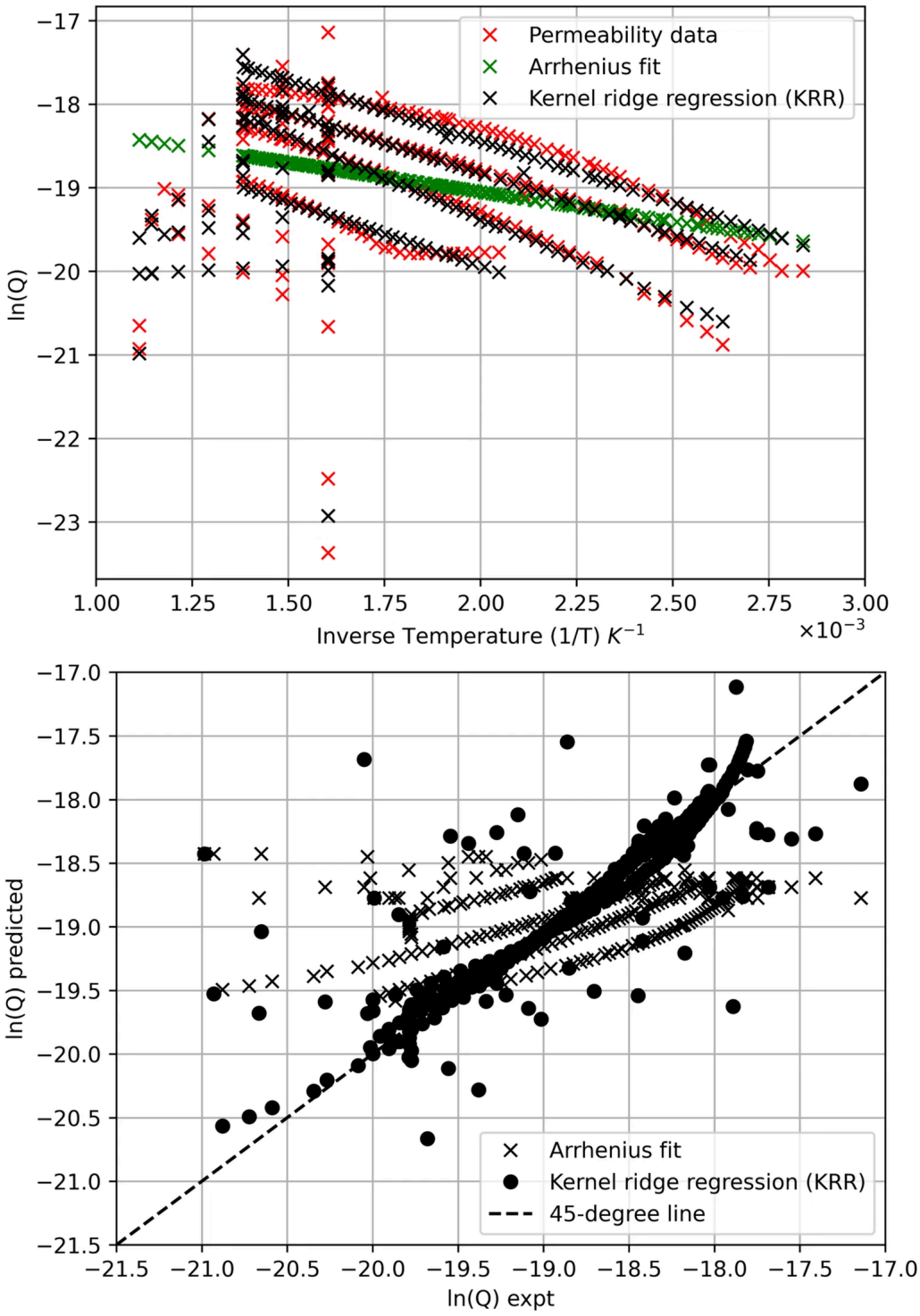

Figure 6. Kernel regression model: (**upper**) model comparison with original data and Arrhenius plot, (**lower**) predicted vs. actual ln permeability plots.

The predictive performance of the KRR model is further illustrated in the lower plot of Figure 6, where $ln(Q)_{pred}$ is plotted against $ln(Q)_{exp}$. Relative to both the Arrhenius and Linear Regression models, the KRR predictions are distributed much closer to the ideal parity relationship $(y=x)$, indicating substantially improved predictive capability. This improvement is reflected by a reduction in the permeability-scale MAPE to 32.15%,

compared with 123.43% and 99.9% for the Arrhenius and Linear Regression models, respectively. On the ln(Q) scale, the KRR model achieved an MAPE of 1.26%, indicating substantially improved prediction of the target variable used during model development. Model performance was further evaluated using five-fold cross-validation, which indicated acceptable prediction reliability for the available dataset.

Finally, the advantage of residual learning was established by estimating the MAPE for permeability predictions using KRR without the Arrhenius model. In this case, the MAPE (after correcting for extreme outliers) reached 47.12%, demonstrating the benefit of a hybrid physics-inspired and data-based model over a purely data-based approach. In addition, to quantify residual inter-study variability, the coefficient of variation of permeability was calculated within narrow composition–temperature windows. For 60 wt% Pd–40 wt% Cu at 670–680 K, this yields a relative uncertainty of approximately 36%, which is considered as a conservative literature-derived error for the dataset. Thus, a mean absolute percentage error of 32.15% is consistent with the inherent inter-study variability of the compiled dataset, indicating that the model approaches the noise floor of the literature data.

Although the Arrhenius baseline was fitted to the full dataset, the resulting parameters ($K_0 \approx 2.18 \times 10^{-8}$ mol m^{-1} s^{-1} Pa$^{-0.5}$ and $E_a \approx 5.85$ kJ mol^{-1}) closely match experimentally reported values for Pd–Cu and Pd–Cu–Ag membranes [7,39], indicating that any information leakage is minimal and that the residual-learning procedure is comparable to the use of a literature-standard baseline.

Figure 7 shows the variation in KRR prediction error with training-set size. The overall decrease in MAE with increasing sample size indicates improved predictive performance as additional permeability data become available. Although local fluctuations are observed, the general trend suggests that the compiled dataset contains useful information for describing permeability behavior across the investigated Pd–Cu membrane systems. Combined with the results shown in Figure 6, the learning-curve analysis provides additional evidence of the predictive capability of the KRR model.

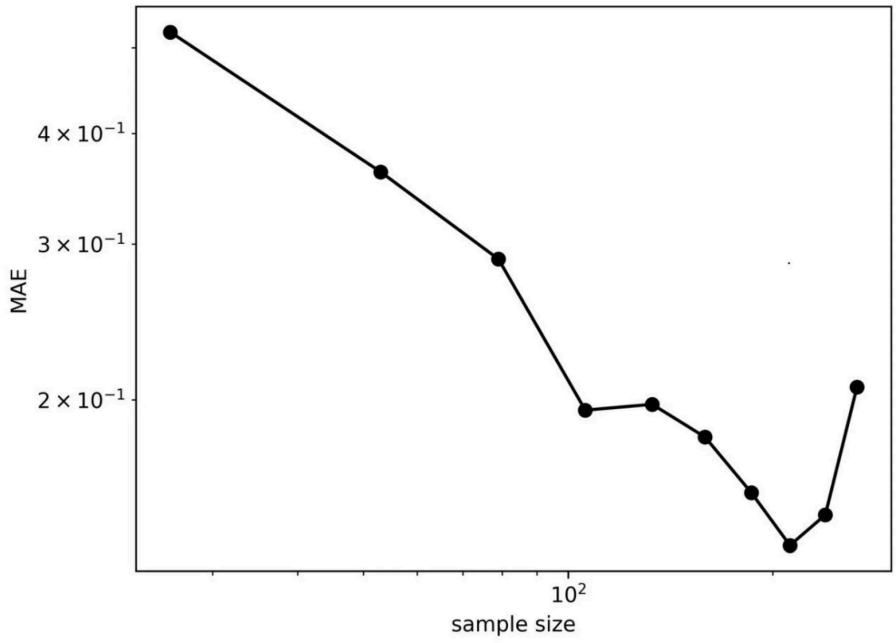

Figure 7. Learning curve (5-fold cross validation error vs. training set size) analysis of the Kernel regression.

It should be noted that the relationships identified by the machine-learning models represent predictive correlations within the compiled dataset and should not be interpreted as direct evidence of underlying transport mechanisms. The physical interpretation of hydrogen transport remains based on established diffusion, solubility, and phase-behavior considerations reported in the literature.

3.5. Practical Applications

The proposed Arrhenius-based residual machine-learning framework can support the development, evaluation, and optimization of Pd–Cu membranes for hydrogen purification. One potential application is in hydrogen purification units (HPUs) integrated with Proton Exchange Membrane Fuel Cell (PEMFC) systems, where a continuous supply of high-purity hydrogen is essential for efficient fuel-cell operation. In these systems, membrane permeability influences hydrogen recovery, product purity, membrane area requirements, and overall process performance. By predicting hydrogen permeability across a range of membrane compositions and operating conditions, the framework can reduce the experimental effort required for permeability characterization and membrane evaluation.

The framework may also be used during the early stages of membrane development. Permeability can be estimated for alternative Pd–Cu membrane compositions and operating conditions similar to those represented in the compiled dataset, allowing candidate membranes to be screened prior to experimental testing. This approach can reduce the number of membranes requiring fabrication and characterization, thereby improving the efficiency of membrane-development efforts.

The model may also support membrane and process-design calculations for hydrogen purification systems. Predicted permeability values can be used to estimate hydrogen flux, membrane-area requirements, hydrogen recovery, and related performance metrics under different operating conditions.

The practical implications of permeability prediction accuracy can be illustrated through membrane sizing for an HPU integrated with a PEMFC stack. The hydrogen consumption rate (n) of a PEMFC stack can be estimated using Faraday's law:

$$n_{H_2} = (N \cdot I \cdot \lambda)/(2\ F) \tag{6}$$

where N is the number of PEMFCs, I is the operating current (A), λ is the hydrogen stoichiometric ratio, and F is Faraday's constant (96,487 C mol^{-1}). Subsequently, the required Pd–Cu membrane area (A) can be estimated using the Sieverts-law relationship:

$$A = \frac{n_{H_2} \cdot l}{Q\left(\sqrt{P_{feed}} - \sqrt{P_{permeate}}\right)} \tag{7}$$

where l is the membrane thickness (m), Q is the hydrogen permeability ($\text{mol m}^{-1}\ \text{s}^{-1}\ \text{Pa}^{0.5}$), and P_i is the hydrogen partial pressures in the feed and permeate sides (Pa). Since the required membrane area is inversely proportional to hydrogen permeability under constant operating conditions, a 32% overprediction of permeability would result in approximately 24.24% underestimation of the required membrane area.

Conversely, a 32% underprediction would lead to approximately 47.06% overestimation. Such deviations have direct implications for membrane sizing, hydrogen supply capacity, and the associated capital costs of the purification unit. This example demonstrates how the prediction accuracy of the proposed model can influence practical engineering design decisions. Such information is valuable during process design and optimization, where multiple operating conditions are typically evaluated prior to pilot-scale implementation.

The proposed framework is intended to support permeability estimation, membrane screening, and preliminary engineering evaluations. Its applicability should therefore be interpreted within the range of membrane characteristics and operating conditions represented in the compiled dataset. Future developments may include integration of the permeability model with membrane degradation and durability assessments. Such an approach would enable simultaneous evaluation of hydrogen transport performance and membrane reliability under relevant operating conditions. Building on previous studies of Pd–Cu membrane degradation, including corrosion-related durability assessments, the proposed framework could be extended to consider both hydrogen permeability and membrane lifetime within a unified predictive framework.

The predictive capability of the present framework is constrained by the information available in the literature-derived dataset. Future studies may benefit from incorporating additional membrane descriptors, including microstructural characteristics such as grain size, phase distribution, and surface-related properties, to further improve permeability prediction.

Further improvement of the model will depend on the availability of additional experimental data covering a wider range of membrane compositions and operating conditions. Expanding the permeability database would improve model robustness and prediction accuracy while allowing the proposed framework to be applied to a broader range of Pd-based hydrogen separation membranes and industrial hydrogen purification processes.

4. Conclusions

An Arrhenius-based residual (Δ) machine-learning framework was developed for predicting hydrogen permeability in Pd–Cu membranes using a literature-derived permeability database. The Arrhenius model successfully described the fundamental temperature dependence of hydrogen permeability but was unable to fully describe the variability present in the dataset, yielding mean absolute percentage error (MAPE) values of 123.4% and 3.08% on the Q and ln(Q) scales, respectively. Residual analysis revealed systematic permeability variations associated with membrane composition, thickness, geometry, and phase that were not captured by the temperature-dependent Arrhenius model.

Modeling the residual contribution through a Linear Regression approach improved predictive performance and reduced the MAPE to 99.9% (2.79% on the ln(Q) scale). However, the remaining prediction errors indicated that the permeability variability could not be fully captured using linear relationships. The Kernel Ridge Regression (KRR) model provided a more accurate representation of the permeability data, reducing the Q-scale MAPE to 32.15% and the ln(Q)-based MAPE to 1.26%. These results indicate the presence of nonlinear interactions among the investigated membrane characteristics and operating-condition variables. Combining Arrhenius transport modeling with machine-learning-based residual prediction improved the prediction of hydrogen permeability in Pd–Cu membranes. Finally, standalone KRR without the Arrhenius model yielded an MAPE of 47.12%, confirming the clear advantage of our hybrid physics-in-

spired residual learning framework over a purely data-based approach.

The developed model may assist membrane evaluation and process design studies by providing rapid permeability estimates for membrane compositions and operating conditions represented within the dataset, thereby reducing the need for extensive experimental evaluation. Although the residual analysis indicated that membrane characteristics contributed to permeability variability, their relative quantitative contributions remain to be evaluated. Future work will focus on extending the present framework by integrating hydrogen transport prediction with membrane degradation and durability models for more comprehensive assessment of Pd-based hydrogen separation membranes.

Supplementary Materials: The following supporting information can be downloaded at: https://www.mdpi.com/article/doi/s1. The Supplementary Materials include the compiled literature-derived dataset used in this study and the Python (v3.11)/Jupyter notebook scripts employed for data processing and model development.

Author Contributions: Conceptualization, H.M.A. and F.A.-H.; Methodology, H.M.A.; Software, E.I.; Validation, F.A.-H.; Formal Analysis, H.M.A., F.A.-H., E.I., and M.A.A.-D.; Investigation, H.M.A.; Resources, F.A.-H.; Data Curation, E.I.; Writing—Original Draft Preparation, H.M.A.; Writing—Review and Editing, F.A.-H., E.I., and M.A.A.-D.; Visualization, E.I. and M.A.A.-D.; Project Administration, H.M.A.; Funding Acquisition, H.M.A. All authors have read and agreed to the published version of the manuscript.

Funding: This research received no external funding.

Institutional Review Board Statement: Not applicable.

Informed Consent Statement: Not applicable.

Data Availability Statement: The data analyzed in this study were compiled from publicly available literature sources cited in the manuscript. Additional processed data supporting the reported results are available from the corresponding author upon reasonable request.

Acknowledgments: This work was carried out during sabbatical leave granted to the author (Hatem M. Alsyouri) from the University of Jordan during the academic year 2023/2024. During the preparation of this manuscript, the authors used Microsoft Copilot (web version accessed July 2026) to assist with improving the organization, clarity, and scientific wording of the manuscript. The authors reviewed, verified, and edited the output as needed and take full responsibility for the content of this publication.

Conflicts of Interest: The authors declare no conflicts of interest.

References

1. Alique, D.; Martinez-Diaz, D.; Sanz, R.; Calles, J.A. Review of Supported Pd-Based Membranes Preparation by Electroless Plating for Ultra-Pure Hydrogen Production. *Membranes* **2018**, *8*, 5. [Google Scholar] [CrossRef] [PubMed]
2. Cerone, N.; Zito, G.D.; Florio, C.; Fabbiano, L.; Zimbardi, F. Recent Advancements in Pd-Based Membranes for Hydrogen Separation. *Energies* **2024**, *17*, 4095. [Google Scholar] [CrossRef]
3. Alentiev, D.A.; Bermeshev, M.V.; Volkov, A.V.; Petrova, I.V.; Yaroslavtsev, A.B. Palladium Membrane Applications in Hydrogen Energy and Hydrogen-Related Processes. *Polymers* **2025**, *17*, 743. [Google Scholar] [CrossRef] [PubMed]
4. Lee, Y.H.; Jang, Y.; Han, D.H.; Lee, S.M.; Kim, S.S. Palladium-Copper Membrane Prepared by Electroless Plating for Hydrogen Separation at Low Temperature. *J. Environ. Chem. Eng.* **2021**, *9*, 106509. [Google Scholar] [CrossRef]
5. Al-Hadeethi, F.F.; Alsyouri, H.M.; Dwairi, S.A. Modeling the Galvanic Corrosion Behavior of PdCu Couple Used in Hydrogen Purification–PEM Fuel Cell Hybrid Systems. *Int. J. Hydrog. Energy* **2016**, *41*, 20771–20778. [Google Scholar] [CrossRef]

6. Howard, B.H.; Killmeyer, R.P.; Rothenberger, K.S.; Cugini, A.V.; Morreale, B.D.; Enick, R.M.; Bustamante, F. Hydrogen Permeance of Palladium–Copper Alloy Membranes over a Wide Range of Temperatures and Pressures. *J. Membr. Sci.* **2004**, *241*, 207–218. [Google Scholar] [CrossRef]
7. Yuan, L.; Goldbach, A.; Xu, H. Segregation and H2 Transport Rate Control in Body-Centered Cubic PdCu Membranes. *J. Phys. Chem. B* **2007**, *111*, 10952–10958. [Google Scholar] [CrossRef] [PubMed]
8. Alraeesi, A.; Gardner, T. Assessment of Sieverts Law Assumptions and 'n' Values in Palladium Membranes: Experimental and Theoretical Analyses. *Membranes* **2021**, *11*, 778. [Google Scholar] [CrossRef] [PubMed]
9. Bosko, M.L.; Dalla Fontana, A.; Tarditi, A.; Cornaglia, L. Advances in Hydrogen Selective Membranes Based on Palladium Ternary Alloys. *Int. J. Hydrog. Energy* **2021**, *46*, 15572–15594. [Google Scholar] [CrossRef]
10. Opalka, S.M.; Huang, W.; Wang, D.; Flanagan, T.B.; Løvvik, O.M.; Emerson, S.C.; She, Y.; Vanderspurt, T.H. Hydrogen Interactions with the PdCu Ordered B2 Alloy. *J. Alloys Compd.* **2007**, *446–447*, 583–587. [Google Scholar] [CrossRef]
11. El-Shafie, M.; Kambara, S.; Hayakawa, Y. Comparative Study on the Numerical Simulation of Hydrogen Separation through Palladium and Palladium–Copper Membranes. *Int. J. Hydrog. Energy* **2022**, *47*, 22819–22831. [Google Scholar] [CrossRef]
12. Goldbach, A.; Yuan, L.; Xu, H. Impact of the Fcc/Bcc Phase Transition on the Homogeneity and Behavior of PdCu Membranes. *Sep. Purif. Technol.* **2010**, *73*, 65–70. [Google Scholar] [CrossRef]
13. Peters, T.A.; Kaleta, T.; Stange, M.; Bredesen, R. Development of Thin Binary and Ternary Pd-Based Alloy Membranes for Use in Hydrogen Production. *J. Membr. Sci.* **2011**, *383*, 124–134. [Google Scholar] [CrossRef]
14. Westerwaal, R.J.; Bouman, E.A.; Haije, W.G.; Schreuders, H.; Dutta, S.; Wu, M.Y.; Boelsma, C.; Ngene, P.; Basak, S.; Dam, B. The Hydrogen Permeability of Pd–Cu Based Thin Film Membranes in Relation to Their Structure: A Combinatorial Approach. *Int. J. Hydrog. Energy* **2015**, *40*, 3932–3943. [Google Scholar] [CrossRef]
15. Martin, M.H.; Galipaud, J.; Tranchot, A.; Roué, L.; Guay, D. Measurements of Hydrogen Solubility in CuxPd100−x Thin Films. *Electrochim. Acta* **2013**, *90*, 615–622. [Google Scholar] [CrossRef]
16. Nayebossadri, S.; Speight, J.; Book, D. Effects of Low Ag Additions on the Hydrogen Permeability of Pd–Cu–Ag Hydrogen Separation Membranes. *J. Membr. Sci.* **2014**, *451*, 216–225. [Google Scholar] [CrossRef]
17. Al-Mufachi, N.A.; Steinberger-Wilckens, R. X-ray Diffraction Study on the Effects of Hydrogen on Pd60Cu40 Wt% Foil Membranes. *J. Membr. Sci.* **2018**, *545*, 266–274. [Google Scholar] [CrossRef]
18. Pushankina, P.; Andreev, G.; Petriev, I. Hydrogen Permeability of Composite Pd–Au/Pd–Cu Membranes and Methods for Their Preparation. *Membranes* **2023**, *13*, 649. [Google Scholar] [CrossRef] [PubMed]
19. Yuan, L.; Goldbach, A.; Xu, H. Real-Time Monitoring of Metal Deposition and Segregation Phenomena during Preparation of PdCu Membranes. *J. Membr. Sci.* **2008**, *322*, 39–45. [Google Scholar] [CrossRef]
20. Yang, J.; Tao, L.; He, J.; McCutcheon, J.R.; Li, Y. Machine Learning Enables Interpretable Discovery of Innovative Polymers for Gas Separation Membranes. *Sci. Adv.* **2022**, *8*, eabn9545. [Google Scholar] [CrossRef] [PubMed]
21. Cao, Z.; Barati Farimani, O.; Ock, J.; Barati Farimani, A. Machine Learning in Membrane Design: From Property Prediction to AI-Guided Optimization. *Nano Lett.* **2024**, *24*, 2953–2960. [Google Scholar] [CrossRef] [PubMed]
22. Bai, X.; Shi, Z.; Xia, H.; Li, S.; Liu, Z.; Liang, H.; Liu, Z.; Wang, B.; Qiao, Z. Machine-Learning-Assisted High-Throughput Computational Screening of Metal–Organic Framework Membranes for Hydrogen Separation. *Chem. Eng. J.* **2022**, *446*, 136783. [Google Scholar] [CrossRef]
23. Kolor, E.; Usman, M.; Boonyubol, S.; Mikami, K.; Cross, J.S. Advances in Palladium-Based Membrane Research: High-Throughput Techniques and Machine Learning Perspectives. *Processes* **2024**, *12*, 2855. [Google Scholar] [CrossRef]
24. Chen, W.-H.; Wu, D.-R.; Chang, M.-H.; Rajendran, S.; Ong, H.C.; Lin, K.-Y.A. Modeling of Hydrogen Separation through Pd Membrane with Vacuum Pressure Using Taguchi and Machine Learning Methods. *Int. J. Hydrog. Energy* **2025**, *140*, 1004–1016. [Google Scholar] [CrossRef]
25. Yang, Y.; Guo, Z.; Gellman, A.J.; Kitchin, J.R. Simulating Segregation in a Ternary Cu–Pd–Au Alloy with Density Functional Theory, Machine Learning, and Monte Carlo Simulations. *J. Phys. Chem. C* **2022**, *126*, 1800–1808. [Google Scholar] [CrossRef]
26. Wu, T.; Zhang, J.; Yan, Q.; Wang, J.; Yang, H. Machine Learning in the Design and Performance Prediction of Organic Framework Membranes: Methodologies, Applications, and Industrial Prospects. *Membranes* **2025**, *15*, 178. [Google Scholar] [CrossRef] [PubMed]
27. Nazari, S.; Abdelrasoul, A. Advancements and Applications of Artificial Intelligence and Machine Learning in Material Science and Membrane Technology: A Comprehensive Review. *Membranes* **2025**, *15*, 353. [Google Scholar] [CrossRef] [PubMed]

28. Grumet, M.; von Scarpatetti, C.; Bučko, T.; Egger, D.A. Delta Machine Learning for Predicting Dielectric Properties and Raman Spectra. *J. Phys. Chem. C* **2024**, *128*, 6464–6470. [Google Scholar] [CrossRef]
29. Mckinley, D.L. Method for Hydrogen Separation and Purification. U.S. Patent 3439474, 22 April 1969. [Google Scholar]
30. Edlund, D.J.; McCarthy, J. The Relationship between Intermetallic Diffusion and Flux Decline in Composite-Metal Membranes: Implications for Achieving Long Membrane Lifetime. *J. Membr. Sci.* **1995**, *107*, 147–153. [Google Scholar] [CrossRef]
31. Roa, F.; Block, M.J.; Way, J.D. The Influence of Alloy Composition on the H2 Flux of Composite Pd-Cu Membranes. *Desalination* **2002**, *147*, 411–416. [Google Scholar] [CrossRef]
32. Roa, F.; Way, J.D. Influence of Alloy Composition and Membrane Fabrication on the Pressure Dependence of the Hydrogen Flux of Palladium−Copper Membranes. *Ind. Eng. Chem. Res.* **2003**, *42*, 5827–5835. [Google Scholar] [CrossRef]
33. Decaux, C.; Ngameni, R.; Solas, D.; Grigoriev, S.; Millet, P. Time and Frequency Domain Analysis of Hydrogen Permeation across PdCu Metallic Membranes for Hydrogen Purification. *Int. J. Hydrog. Energy* **2010**, *35*, 4883–4892. [Google Scholar] [CrossRef]
34. Matsumura, Y. A Basic Study of High-Temperature Hydrogen Permeation through Bcc Pd–Cu Alloy Foil. *Sep. Purif. Technol.* **2014**, *138*, 130–137. [Google Scholar] [CrossRef]
35. Iype, E.; Urolagin, S. Machine Learning Model for Non-Equilibrium Structures and Energies of Simple Molecules. *J. Chem. Phys.* **2019**, *150*, 024307. [Google Scholar] [CrossRef] [PubMed]
36. Yun, S.; Ted Oyama, S. Correlations in Palladium Membranes for Hydrogen Separation: A Review. *J. Membr. Sci.* **2011**, *375*, 28–45. [Google Scholar] [CrossRef]
37. Alimov, V.N.; Busnyuk, A.O.; Notkin, M.E.; Peredistov, E.Y.; Livshits, A.I. Hydrogen Transport through V–Pd Alloy Membranes: Hydrogen Solution, Permeation and Diffusion. *J. Membr. Sci.* **2015**, *481*, 54–62. [Google Scholar] [CrossRef]
38. Rodriguez, C.C. *The Kernel Trick [Online]*; Department of Mathematics and Statistics, University at Albany: Albany, NY, USA, 2004; pp. 1–5. Available online: https://omega0.xyz/omega8008/machine-learning-dir/notes-dir/ker1/ker1.pdf (accessed on 1 July 2024). [Google Scholar]
39. Zhao, L.; Goldbach, A.; Bao, C.; Xu, H. Structural and Permeation Kinetic Correlations in PdCuAg Membranes. *ACS Appl. Mater. Interfaces* **2014**, *6*, 22408–22416. [Google Scholar] [CrossRef] [PubMed]

Disclaimer/Publisher's Note: The statements, opinions and data contained in all publications are solely those of the individual author(s) and contributor(s) and not of MDPI and/or the editor(s). MDPI and/or the editor(s) disclaim responsibility for any injury to people or property resulting from any ideas, methods, instructions or products referred to in the content.